Petroleum Research xxx (xxxx) xxx

Contents lists available at ScienceDirect

Petroleum Research

journal homepage: http://www.keaipublishing.com/en/journals/petroleum-research/

Full Length Article

Modeling displacement flow inside a full-length casing string for well cementing

Hu Dai [a, *], Ali Eslami [b], Jason Schneider [c], Gefei Liu [a], Fred Schwering [d]

[a] Pegasus Vertex, Inc., USA
[b] Laval University, Canada
[c] Sanjel Energy Services, Canada
[d] Athabasca Oil Corporation, Canada

ARTICLE INFO

Article history:
Received 16 February 2023
Received in revised form
14 August 2023
Accepted 14 August 2023
Available online xxx

Keywords:
Inside pipe displacement
Displacement efficiency
Numerical model
Primary cementing
Displacement flow

ABSTRACT

While computer modeling of annular displacement efficiency is widely applied in cementing engineering, modeling the displacement flow inside a casing or drill string for cementing operations has received less attention. Although predicting displacement efficiency inside a full-length pipe is desired by cementing engineers, the attempt of developing a model with both efficiency and accuracy faces challenges. Access to computer simulators for this purpose is limited. Compared with annular flow, the displacement flow inside pipe, although within a simpler geometry and without eccentricity effect, is not simpler in physics, modelling strategy and predictability, because a variety of flow patterns and flow instabilities can develop to create complicated fluid interfaces. In this paper, we present an integrated numerical model developed to simulate displacement flows inside a full-length pipe, which connects an existing annulus model to enable complete displacement simulations of cementing jobs. The model uses three-dimensional grid to solve fluid concentrations with degrees of mixing, and incorporates flow instability detection and flow regime determination. Applied in cementing, the model accounts for effects of pumping rate, well inclination, pipe rotation, fluid densities, rheological parameters and more. This computationally efficient model does not rely on high-resolution mesh as often required by conventional Computational Fluid Dynamics models, thus it is suitable to be implemented in a cementing software for daily use by well cementing engineers. The methodology of the model is discussed in detail in this paper. To validate the model, we examine simulation results against experimental results obtained in our laboratory tests and CFD simulations; acceptable agreement is found under different testing conditions. We also presented two case studies of real cementing jobs with cement evaluation logs compared to simulation results, showing that the model can predict consistent displacement efficiency results.

1. Introduction

Displacement flow is a type of internal flow through a duct of specific geometry (commonly in pipe or in annulus) involving two or more fluids, driven by an imposed velocity or pressure difference. This type of flow is seen and utilized in many different industries, such as manufacturing, food processing, and petroleum industry (Nelson and Guillot, 2006; Amiri et al., 2016). In drilling engineering, displacement flows of interest can take place in pipe, annulus or in the reservoir. In well cementing, displacement efficiency including inter-fluid contaminations directly affect the set cement quality, the top of cement (TOC) and the life of well (Tehrani et al., 1992). Because a larger number of parameters than the single-phase flow is involved, complex phenomena arise from the interface evolution and fluid mixing (Etrati and Frigaard, 2018b); therefore, predicting this type of flow is difficult. For example, the well inclination angle can strongly affect the flow pattern because of the buoyance force arising from the density difference of the fluids.

Many research works have been done in recent years with respect to annulus displacement efficiency, including experimental

* Corresponding author.
E-mail address: hdai@pvisoftware.com (H. Dai).

https://doi.org/10.1016/j.ptlrs.2023.08.004

studies (e.g., Moran and Savery, 2007; Deawwanich, 2013; Renteria et al., 2018; Skadsem et al., 2019; Eslami et al., 2022) and numerical studies (e.g., Braghini et al., 2010; Ermila et al., 2012; Feng et al., 2013; Enayatpour and van Oort, 2017; Foroushan et al., 2018; Wang and Dai, 2018; Kiran et al., 2019; Skadsem et al., 2019; Sarmadi et al., 2022). The industry and academia have established a few computer simulators for annular displacement flow (Bittleston et al., 2002; Pks and Yerubandi, 2010; Chin and Zhuang, 2011; Aranha et al., 2012; Chen et al., 2014; Grasinger et al., 2015; Tardy and Bittleston, 2015; Xie et al., 2015; Dai and Liu, 2017; Maleki and Frigaard, 2017; Tardy et al., 2017). Understanding of the annular displacement flow and the strategies for improving annular displacement efficiency are thus greatly improved (Liu, 2021). However, much less attention was paid to the inside-pipe displacement. On one hand, this is because the cement sheath and cement bond are more directly associated with annular efficiency, which is sensitive to pipe eccentricity and wellbore irregularity (e.g., Enayatpour and van Oort, 2017; Kiran et al., 2019; Skadsem et al., 2019; Sarmadi et al., 2022); and on the other hand, one can largely prevent slurry contaminations during the displacement inside casing by using mechanical separators including bottom and top plugs, thus the concern is avoided. However, a capability of simulating displacement efficiency inside the casing or drill string is still frequently demanded when separators are not used and fluid mixing is influential in both primary and plug cement placement.

Although many of the physical and modelling concepts are shared between annulus and in-pipe displacement flows, it is necessary to develop different techniques to model the flow inside a pipe (Tardy et al., 2017). Compared with annular flow, the flow inside a pipe, although with simpler geometry and without eccentricity effect, is however not simpler in physics, modelling strategy and predictability, because of flow instabilities and lots of possible flow patterns as found in many experimental studies (e.g., Etrati et al., 2018). However, very few of the aforementioned simulators have incorporated the simulation capability for in-pipe flows. In addition, the actual displacement process in a real casing or drill pipe is not directly measurable, because acoustic logging methods account for only final displacement results in the annulus; therefore, a full-length displacement model for pipe flow could not be easily calibrated or verified using field measurement.

Cementing engineers are often dealing with non-Newtonian fluids, as drilling fluids and cement slurries are; however, a study of simpler Newtonian displacement flow can greatly benefit the understanding of more complicated flow in cementing. Newtonian displacement flow has the simplest rheology; however, the flow is not ordinary. Complex flow behaviors emerge because of instability and transverse buoyancy effects. Taghavi et al. (2011, 2012b), Alba et al. (2012, 2013a), and Amiri et al. (2016) studied iso-viscous density-stable and density-unstable displacement flows experimentally. Dimensionless parameters are introduced to attribute a flow to one of three regimes: diffusive, viscous and inertial types. This classification is not strict and more sub-patterns exist. On the other hand, instabilities due to viscosity contrast are also studied using analytical, experimental and numerical approaches for density-stable, unstable and non-buoyant flow (Joseph et al., 1984; Selvam et al., 2009; Taghavi et al., 2012a; Etrati et al., 2018; Etrati and Frigaard, 2018a,b), when the fluid interfaces take different forms such as wavy, cyclic, stable, inertia or mixed patterns (Etrati et al., 2018). Predicting flow instabilities is a very complicated task; however, it is also a necessary step in tracking the development of displacement flow and predicting displacement efficiency. When Newtonian flows are not adequately understood, the non-Newtonian flows are even more mysterious because not many studies have been conducted (examples: Alba et al. (2013b); Etrati et al. (2018)).

In the stable flow of homogeneous Newtonian fluid inside a pipe, a fluid interface will move forward in a stretching parabolic shape. The axisymmetric interface evolution is accurately predictable. The challenge comes when the symmetry breaks by transverse buoyancy and by a variety of flow instabilities, which create complicated three-dimensional (3D) patterns. Both mathematical analysis and numerical solution of the flow are difficult. Modern numerical techniques of computational fluid dynamics (CFD) can accurately solve the 3D flow in a complex geometry with highly refined mesh; however, solving the flow in a full-length pipe in cementing application using a CFD solver is mostly infeasible owing to the high computational cost. Numerical simulations using CFD are performed mainly for research purpose and often for a short section of pipe or annulus only (Etrati and Frigaard, 2018b; Wang and Dai, 2018). Industrial development of CFD solutions for practical cementing applications is also very limited.

Cementing simulators using reduced-order models for displacement efficiency have been largely focused on annulus flow only. This type of models is often based on 2D simplification such as lubrication assumption, given that the annulus gap is small compared to the casing or hole diameter (e.g., Aranha et al., 2012; Xie et al., 2015; Maleki and Frigaard, 2017; Tardy et al., 2017). This type of method is not applicable for modeling the flow inside a pipe. Tardy et al. (2017) introduced a simplified in-pipe model, which was implemented in an industrial cementing simulator. In that model, concentric, segregated and mixed flow regimes are considered. Concentric flow is present when transverse velocity and forces are insignificant; segregated flow regime takes place wherever the transverse buoyancy is big enough to overcome viscous-force driven central flow; mixed flow emerges when instabilities are detected such that fluids are mixed to form a homogenous mixture. Two types of instabilities, Kelvin-Helmholtz (K—H) instability and Roll-wave instability, are considered. Because only limited information on this model is published, the degree of accuracy of this model under different well and flow conditions is unknown. Besides, this model does not fully resolve all flow regimes such as partial mixing and non-concentric flow; the onset conditions of the instabilities are also not discussed.

In this paper, we present a novel computer model using three-dimensional grid suitable for simulating displacement flow in a full-length pipe for well cementing applications. The model allows flow regime and instability detection, but avoids use of high-resolution mesh, thus improves computational efficiency desired in cementing job designs. We explain the method, simulation results, experimental results for validations, and we show applications of the model in case studies.

2. Material and methods

A basic two-miscible fluid displacement problem in a pipe involves several governing parameters: inlet velocity, inclination angle of the pipe, densities of fluids, rheological parameters of fluids, internal diameter and length of the pipe, rotational speed for rotating pipe, and molecular diffusivity of fluids (ignored in this model). For practical applications, however, the model must deal with more than two fluids and variable inclination angles and pipe diameters. The present computer model does not aim at precisely solving 3D flow field and fluid transport as conventional CFD models do, instead it uses major simplifications in the solution process. The model has two advantages over the conventional CFD models. First, it greatly improves the computational efficiency by avoiding solving large linear system (such as Poisson equation); second, it is developed to solve the field-scale pipe flow with a large length-to-diameter ratio (~ 10^4), for which conventional CFD

model is difficult or impossible to mesh and solve. The accuracy is compromised; however, it is suitable to be implemented in engineering applications. This model integrates a number of innovative approaches as discussed in the following.

2.1. Flow regime

The current model considers stratified flow and non-stratified flow, both of which can develop partial mixing. Fluid mixing is tracked and quantified in 3D grid (Fig. 1). Various flow patterns are "naturally" formed by solving fluid fraction transport through a volume of fluid (VOF) method; except that two regimes are determined by additional process: stratified flow is resulting from an artificial process of "fluid segregation", and fully mixed flow is applied after physical instability is detected.

2.2. Mesh

The velocity, pressure and fluid concentrations are defined on the 3D structured grid. Two-dimensional plane mesh is created in each axial position along measured depth (MD). We consider two candidates of plane meshes to fit different patterns of displacement flow, as shown in Fig. 2a and b. Although the concentric mesh is convenient in describing concentric flows, it has difficulty to represent stratified flows, for which the stratified mesh (Fig. 2b) is advantageous. The concentric mesh was used in a previous model, and the latter is used in the current model. This type of grid has *horizontal* lines and longitudinal lines, and the longitudinal line in the middle is aligned with the projection of gravity vector in the cross section. Note that in a horizontally laid pipe, the central longitudinal grid line coincides with the gravity vector; and in a vertical pipe, that grid line becomes horizontal in space and its direction is not uniquely defined.

2.3. Axial velocity

Corresponding to each axial position, two types of axial velocity profiles are considered: concentric profile and stratified profile. Whenever flow is stratified, a stratified velocity profile is solved; in other cases, concentric profile is solved. We consider Hershel-Buckley rheological model, a generalized non-Newtonian model, which has a constitutive relationship written as

$$\begin{cases} \tau = \tau_o + k(\dot{\gamma})^n, \text{if } \tau > \tau_o \\ \dot{\gamma} = 0, \text{if } \tau \le \tau_o \end{cases} \quad (1)$$

Where $\dot{\gamma}$ is the shear rate, τ is the shear stress, τ_o is the yield stress, k is the consistency index, and n is the flow index. For conciseness, the formulation of concentric axial velocity profile is present in Appendix A.1. When stratified velocity profile is considered, which is more complicated, the velocity distribution along the vertical centerline is first found numerically. This process is similar to that for the concentric profile but it considers different fluids at each horizontal layer, thus iterative procedure is needed. Then velocity distribution in each layer is solved and adjusted (see Appendix A.1). Fig. 3a–c illustrates the cross section grid, a cell of finite volume, and an example of computed vertical velocity profile, respectively. This method for solving velocity profile is only an approximation, but the computation is fast and suitable for solving the segregated flow for engineering applications. Its accuracy is discussed in Section 3.1.

2.4. Fluid transport

A numerical technique based on the classic "volume of fluid" method in CFD is used for solving the time dependent fluid fraction inside pipe, similar to the method developed for the annulus model in Dai and Liu (2018). With a finite volume discretization, the method solves the following equation in three-dimensional space:

$$\frac{\partial f_i}{\partial t} + \mathbf{u} \cdot \nabla f_i = \mathrm{D_m}\, \nabla^2 f_i \quad (2)$$

where f_i is the volume fraction of the i-th fluid, $\mathbf{u}$ is the velocity vector, and the $\mathrm{D_m}$ is the macroscopic diffusion coefficient induced by interfacial instability or turbulence. The numerical method for solving Eq. (2) is introduced in Appendix A.2. In solving Eq. (2), we ignore the term on the right hand side, meaning that fluid mixing due to instabilities and diffusion is not considered in this step, because incorporating it into a numerical model will require substantial increase of the model fidelity. An ideal fluid interface is stretched by non-uniform velocity but remains sharp, which is captured in this first step. However, in order to construct a reasonable representation of the fluid interfaces and concentration field, several approaches are designed in this model to handle fluid mixing and segregation, and to track mixed fluids in flow (see Appendix A.3-A.5).

2.5. Pipe rotation

Rotation of the pipe significantly influences the characteristics of displacement flow in the annulus and in the pipe. Because of the coupling of axial and azimuthal velocities, which creates three-dimensional helical flow, it is difficult to quantify the impact of pipe rotation in a coarse numerical model, especially for non-Newtonian fluid flow. Because transverse velocity is not solved in current model, the effect of rotation is considered only in the process of fluid segregation and fluid mixing. The fluid segregation is deactivated if rotational flow is strong enough, i.e., when rotational speed of the pipe exceeds the buoyant inertial velocity:

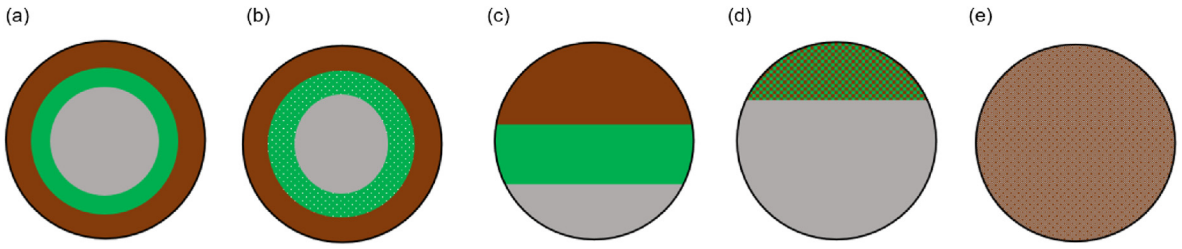

Fig. 1. An illustration of various flow regimes possible in the displacement flow (cross section views). Three fluids are considered in this illustration but more fluids are allowed in the model. Mud, spacer and cement are represented by brown, green and gray colors, respectively. (a) Concentric flow; (b) concentric flow with mixed middle layer; (c) stratified flow; (d) stratified flow with mixed top layer; (e) fully mixed flow. This illustration shows only a few featured patterns, while the current model handles more complicated, arbitrary flow patterns.

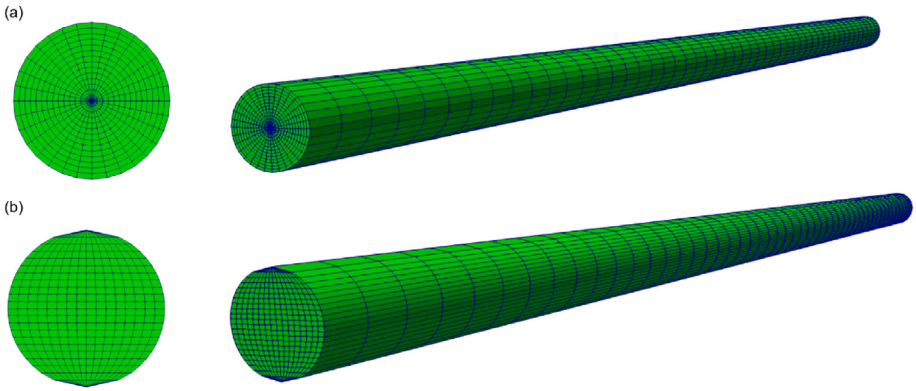

Fig. 2. The (a) structured 3D grids and cross-section meshes used in the model. (a) Concentric grid, (b) stratified grid.

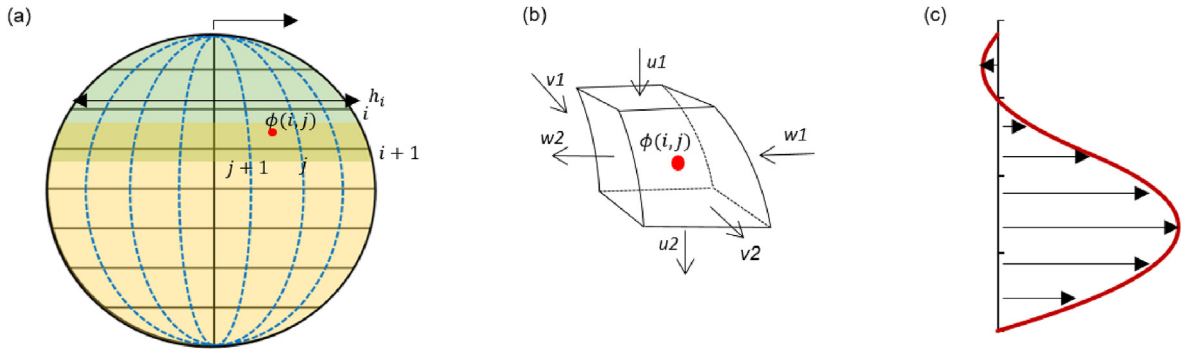

Fig. 3. Illustration of the numerical method. (a) A stratified cross section mesh with straight "horizontal lines" and vertical "longitudinal lines". (b) A 3D finite volume cell used in the current model with the flow-in and flow-out velocities drawn on all faces. (c) An example of axial velocity profile along the vertical central line.

$$v_r = \omega R > v_t \tag{3}$$

where the inertial velocity v_t is defined as

$$v_t = \sqrt{At\, g \sin\beta\, D}\,. \tag{4}$$

Where, *At* is Atwood number, g is gravity acceleration, β is inclination angle, D is the pipe diameter. The Atwood number *At* is defined as

$$At = \frac{\rho_h - \rho_l}{\rho_h + \rho_l}, \tag{5}$$

where ρ_h and ρ_l are densities of heavy fluid and light fluid.

Furthermore, when we check instabilities, the Reynolds number of imposed flow is corrected to the following:

$$Re = \frac{\rho D}{\mu}\sqrt{u_0^2 + v_r^2} \tag{6}$$

3. Results and discussion

Our model has been implemented in a computer program to allow simulating displacement efficiency for cementing jobs. The program can run with variable grid resolution and time step size according to numerical stability and accuracy requirements for short or long pipes, with different sections of diameters and real survey data. To validate the proposed model, we performed CFD simulations and laboratory tests of two-fluid displacement flows, as will be discussed in section 3.1 and 3.2. Additional numerical studies and field applications are discussed in section 3.3 and 3.4.

3.1. Comparison with CFD simulations

Modeling displacement flow using OpenFOAM (Weller et al., 1998) represents a standard CFD approach to solve for the displacement efficiency. Three cases are presented here. They are Newtonian displacement flow in a nearly horizontal pipe (inclination angle is 83° from the vertical). The pipe is 4 m in length and 19 mm in diameter. The displacing fluid is 1020 kg/m3 and the displaced fluid is 1000 kg/m3. The viscosity is 1 cP for both fluids. The initial interface between the two fluids is in the middle of the pipe, or 2 m from either end. In the CFD model, the flow domain is discretized to 34000 cells with thinner layers near the wall, and the computational time is 1~2 h depending on particular cases; the current model used a 100 × 13 × 18 mesh (23400 cells in total), and the computational time for a simulation is approximately 2 min. Both models run on a regular PC (Intel® Core™ i7-6600U@ 2.6 GHz 2 Cores, 8.0 GB RAM, running Windows 10). Three cases have different imposed velocities. Fig. 4 is a comparison of solved velocity profiles at specified times and locations of two-fluid regions from both CFD model and the current model, and Fig. 5 is a comparison of fluid concentrations in the vertical central plane simulated using both models.

The CFD model and the current model produced similar velocity profiles. Within the circular cross section, the flow is symmetric with respect to the vertical centerline. When the imposed velocity is small, a significant reversed flow is found within a large region in the top of the cross section. With a higher imposed velocity, the

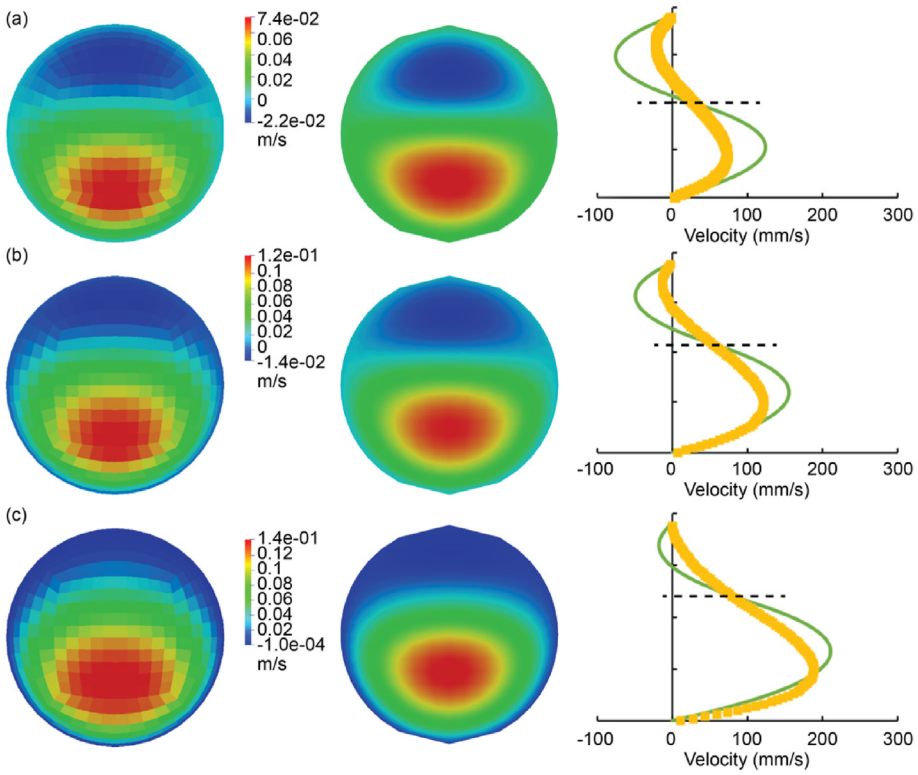

Fig. 4. Velocity profiles of two-fluid displacement flow for three cases with different imposed velocities in a pipe. From top to bottom, the imposed velocity is (a) 18.7 mm/s (the axial position is 0.5m after the initial separation and the time is 56 s, Re = 360, Fr = 0.42), (b) 42 mm/s (1 m after separation position and at 32 s, Re = 810, Fr = 0.95), and (c) 76 mm/s (1.5 m after separation position and at 21 s, Re = 1463, Fr = 1.72). The left column: the velocity contours in the cross section by CFD model, where red color indicates high velocity and blue indicates low or negative velocity (negative values mean reversed flow). The middle column: results by the current model at the same times and locations as in the left column. The right column: a comparison of velocity profiles along the vertical centerline, where green lines are results from the current model and yellow lines from the CFD model. The black dashed lines indicate the interface positions between the displaced and displacing fluids predicted by the current model. Interfaces in the CFD results are much more diffusive and thus not clearly defined; therefore, they are not shown in the plots. Because of different grid structures, contours from CFD model (left column) are not smoothly visualized as those from the current model (the middle column).

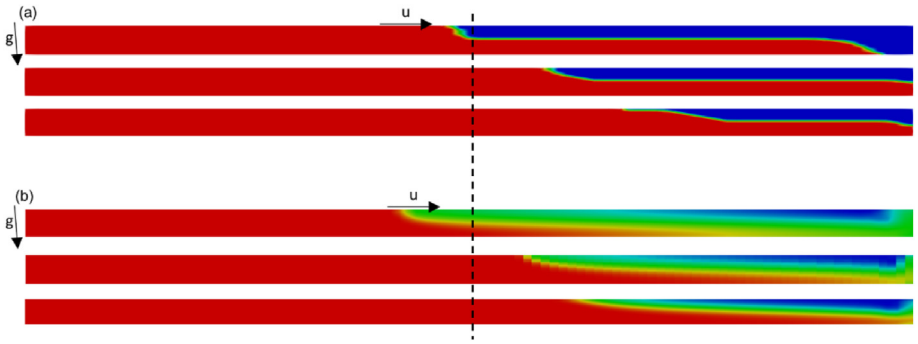

Fig. 5. Fluid concentration within the central plane. The displacing fluid is shown in red and the displaced fluid in blue. Colors between red and blue indicate mixing of the two fluids. The flow direction is indicated by the arrow with label *u* and the gravity direction is indicated by *g*. (a) Results from the current model; (b) results from CFD simulations. In both (a) and (b), three cases from top to bottom have imposed velocities of 18.7 mm/s, 42 mm/s, and 76 mm/s. Times corresponding to the snapshots of the cases are 56s, 32s and 21 s after imposing the flow from the left end. Dashed line indicates the position of the initial separation of displacing and displaced fluids. Note a constant diffusivity of 10^{-6} m2/s was assumed in the CFD simulations, which resulted in the diffusive fluid interfaces.

negative flow region largely shrank, and thus the forward flow is dominant. The velocity profiles along the vertical centerline more clearly show this trend (right column of Fig. 4). Note the maximum and minimum velocities are not accurately matched between the results of current model and the CFD model, although the shapes of contours are similar. This is especially pronounced at a small imposed velocity. A possible explanation of this discrepancy is that the velocity results of the present model are found after a sharp segregation between the two fluids is predicted, while the results in CFD reveal significant intermixing near the interface, which is clearly seen in Fig. 5. We show the simulation results on the central plane along axial direction for the same cases in Fig. 5. At 18.7 mm/s, a back flow of displaced fluid exists on the top, and the trailing front of the interface thus moves to the upstream of the initial separation point. At a higher imposed velocity, although local negative velocity still exists inside the two-layer region, all displaced fluid is gradually displaced to the downstream. The two models produced consistent results; but the results from CFD show

significant mixing at the interface, while the current model sees clear fluid segregation.

3.2. Comparison with experimental results

We have performed laboratory tests to validate the present model. The experimental setup and test procedures are explained in Appendix B. In this section we present a few simulations against experimental results. In the first two cases, we examine a vertical pipe displacement flow for density-unstable Newtonian flows. The density of displaced fluid (998 kg/m^3) is lower than that of the displacing fluid (1000 kg/m^3) whereas both fluids have the same viscosity (1 cP). The current experimental work presents that the stability of this type of flow is affected by the imposed flow rate which is in line with previous studies (e.g., Amiri et al., 2016). The experimental and simulation snapshots are shown in Fig. 6, representing a vertical pipe of 805 mm in length after the gate valve (initial separation of fluids). We compare the impact of imposed velocity for iso-viscous Newtonian displacements for two different flow rates: 61.9 mm/s in Figs. 6a and 10.2 mm/s in Fig. 6b. At higher imposed velocity, the simulation predicts a stable flow with a smooth and clear fluid interface stretching downward, consistent with the experimental results. However, at much lower velocity, we observe unstable flow with mixed fluid front and distorted stream from the laboratory result (left in Fig. 6b), and similar flow features are captured in the simulation (right in Fig. 6b).

In another comparison, we change the fluid densities to investigate the influence of buoyancy on the flow stability. Fig. 7 shows these effects for Newtonian displacements, in which the Atwood number is increased from 0.0001 to 0.07, while the rest of the parameters are fixed. It means that at the same imposed velocity of 54 mm/s, the density of displacing fluid is changed to create three different density contrast cases. The experimental and numerical results for Atwood number of 0.0001, 0.01 and 0.07 are displayed in Fig. 7a, b and c, respectively. At a small Atwood number of 0.0001, the fluid interface is clear in both experimental and simulation results. When the Atwood number increases to 0.01, a slightly wavy and blurred interface is observed in the experimental images, as a consequence of intensified mixing due to instability. Further increase of the Atwood number leads to enhanced transverse mixing. The velocity of the fluid front is thus slowed down, which contributes to an improved displacement efficiency. As can be seen, the numerical model reproduces this trend satisfactorily.

We now look at the viscoplastic displacement flows in a near-horizontal pipe as the third comparison. The pipe is inclined at 83° from vertical. We use a heavy Newtonian fluid of 1039 kg/m^3 to displace a lighter Hershel-Buckley fluid of 998.5 kg/m^3. Note that the yield stress of the displaced fluid is 4.1 Pa which was measured using a DHR-3 TA Instrument rheometer. The experimental results for both a stationary pipe (0 rpm) and a rotating pipe (40 rpm) are shown in Fig. 8a and b. Without rotation, the flow is well segregated (Fig. 8a top and bottom). The experimental result shows a slightly wavy horizontal interface, while the simulation predicts a smoother interface. The tip of displacing fluid by the simulation is slightly falling behind that observed in the laboratory snapshots. When a rotation is applied to the pipe, the fluid segregation breaks, as seen from both laboratory and simulation results in Fig. 8b. The front of displacing fluid is mostly seen flowing near the pipe center in the simulation, and however, it is more distributed to the near-wall region in the laboratory result.

3.3. Full-length pipe

We simulate a series of cases to verify the usability of the new model for full-length pipes. The length of pipe is 5000 ft (1524 m) and the inner diameter is 5 inch (127 mm). Results of three cases from the current model and from a previous model are presented in Fig. 9. The previous model uses an axisymmetric mesh to solve symmetric flow and does not consider flow regimes, thus the influences of buoyancy effect and flow instabilities are not included. We name this previous model “concentric model” hereafter. All snapshots in Fig. 9 are corresponding to the time when a volume of fluid equal to a half of the pipe's interior volume is pumped. The first and second cases (Fig. 9a and b) show the effect of density difference in a vertical pipe. When a low-density fluid displaces a high-density fluid (Case 1), it creates stable, symmetric flow, as predicted by both models. When a high-density fluid displaces a low-density fluid (Case 2), different results are seen, where the current model predicted unstable fluid interface. The instability helped reduce the length of stretching, thus improved the displacement efficiency. For the flow in a horizontal pipe (Case 3 in Fig. 9a and b), the current model predicts fluid segregation with the

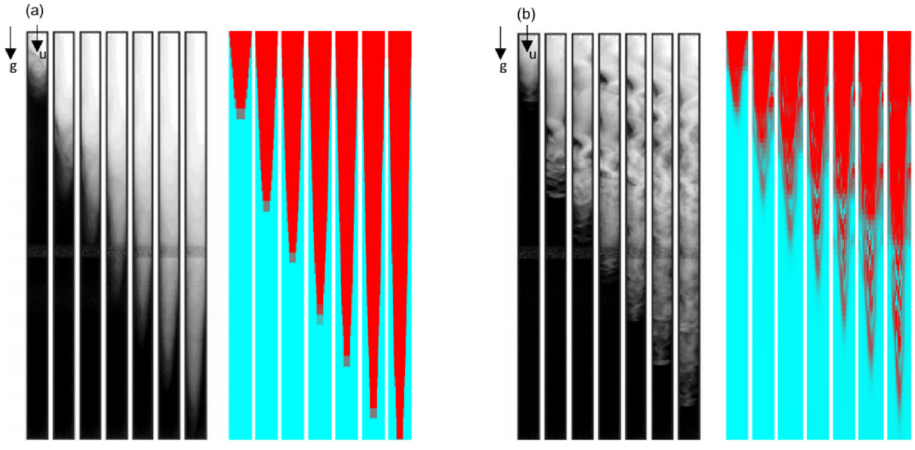

Fig. 6. A comparison between the experimental results (left in both (a) and (b)) and simulations using the current model (right in (a) and(b)) showing the effect of inertia on flow instability in a vertical pipe. The arrows in the figure indicate the gravity vector. The experimental results show the fluid concentrations captured by the camera, in which the white fluid is displacing fluid and the black fluid is the displaced fluid. The simulation results (color images) show the fluid concentrations in the central plane through the pipe axis, in which the red and cyan fluid are displacing and displaced fluids, respectively. (a) Stable flow at imposed velocity $u_0 = 61.9$ mm/s, $\rho_2 = 1000\ kg/m^3$, $\rho_1 = 998\ kg/\ m^3$, $\mu_1 = \mu_2 = 0.001\ Pa.s$, D = 9.6 mm. The Reynolds number Re = 594, and the Froude number Fr = 6.38. (b) Unstable flow at imposed velocity $u_0 = 10.2$ mm/s. Re = 98, Fr = 1.05. The time of each snapshot in (a) and (b) are 1.6, 3.2, 4.1, 5, 5.7, 6.6, 7.3s, and 8.5, 16.7, 21, 25.2, 29.5, 33.5, 37.7s, respectively. The mean shear rates for the flows in (a) and (b) are 6.45 and 1.06 s^{-1}.

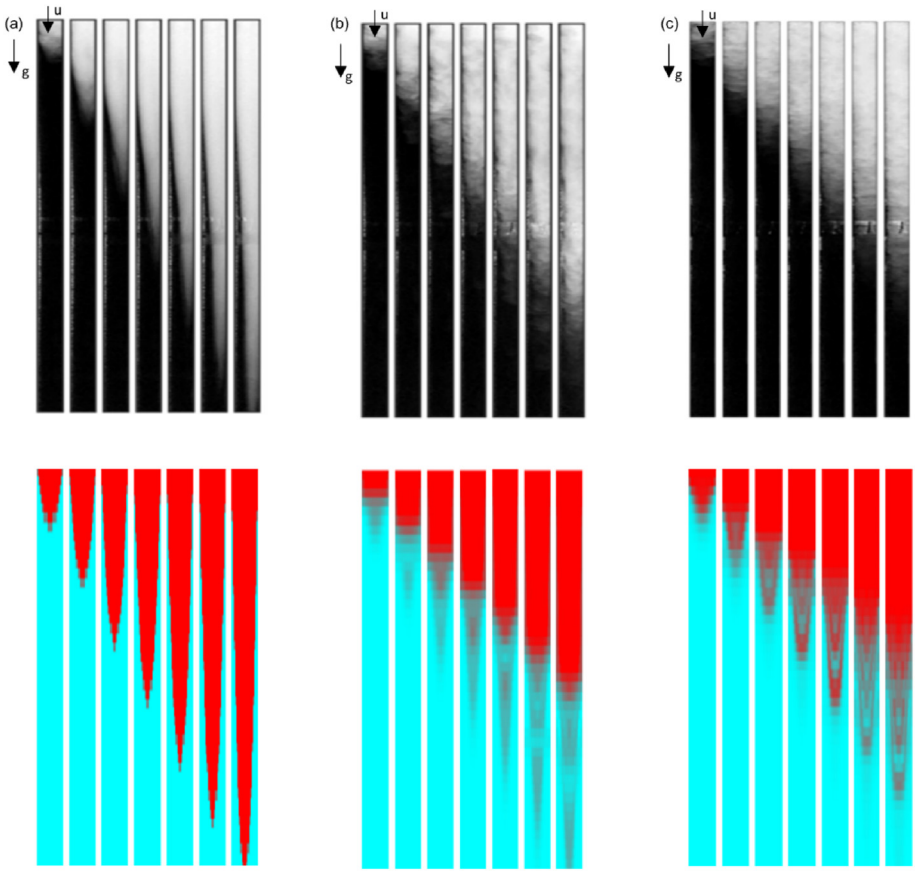

Fig. 7. A comparison between numerical simulations (bottom) and previously published experiment results (top) (Amiri et al., 2016) for three cases of different Atwood number (At). (a) At = 0.0001, Re = 517, Fr = 17.6; (b) At = 0.01, Re = 522, Fr = 1.76; (c) At = 0.07, Re = 556, Fr = 0.66. The imposed velocity is 54 mm/s for all three cases causing a shear rate of 5.62 s^{-1}. The times are 1.25, 2.5, 3.75, 5, 6.25, 7.5, 8.75 s in each plot.

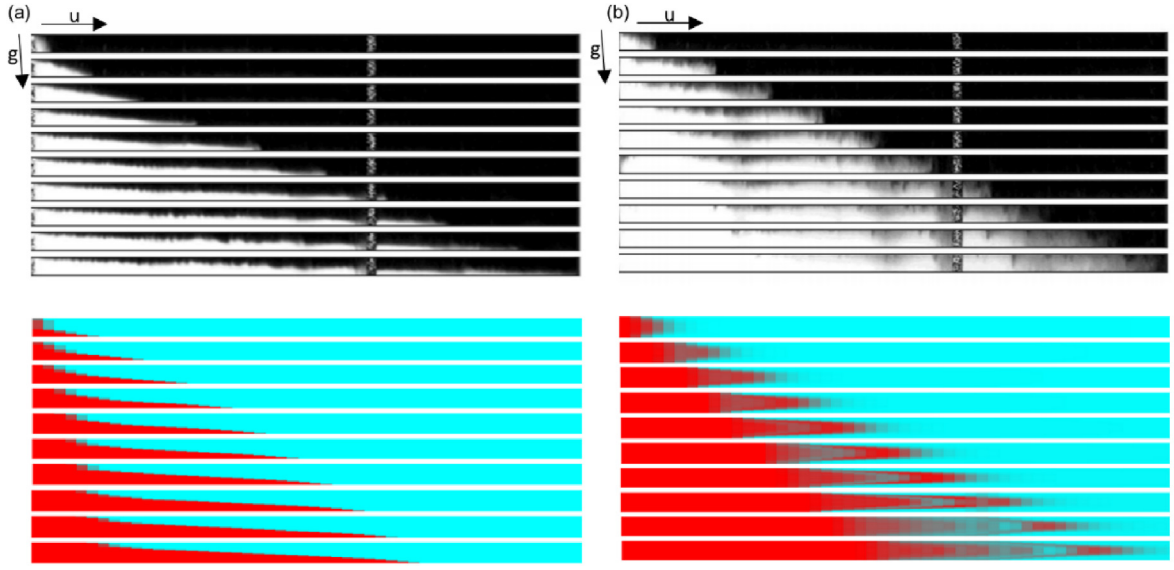

Fig. 8. A comparison of simulation and experimental results for Hershel-Buckley fluid in a near horizontal pipe (β = 83°). In both cases, ρ_2 = 1039 kg/m^3, ρ_1 = 998.5 kg/m^3, μ_2 = 0.001 $Pa.s$, $\tau_{y,1}$ = 4.1 Pa, k_1 = 7.8 $Pa{\cdot}s^n$, n_1 = 0.38, D = 19.05 mm, and imposed velocity u = 47.5 mm/s. (a) Re = 905, Fr = 0.78, Bn = 0.37, m = 6071, No rotation; times are [1.4, 3, 4.6, 6.2, 7.8, 9.4, 11, 12.6, 14.2, 15.8] s. (b) Rossby number = 1.14 (40 rpm), Re = 867, Fr = 0.75, m = 6263. Times are [2.6, 5.4, 8.2, 10.8, 13.6, 16.4, 19, 21.8, 24.6, 27.4] s. The length of pipe in each snapshot is 2000 mm.

displacing fluid moving on top of the native fluid with an almost linearly developing thickness, while the concentric model produces only symmetric flow.

Next, we simulate displacement of Bingham Plastic (BP) fluids

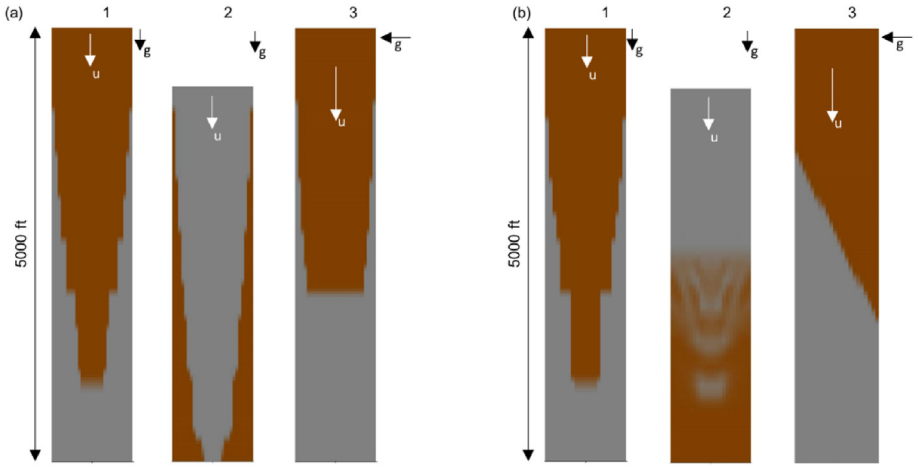

Fig. 9. Three cases simulated by the concentric model (a) and the current model (b). The brown fluid is 1078.3 kg/m3 and the gray fluid is 1437.8 kg/m3. In Case 1 and 2, we simulate flow in a vertical pipe at a flow rate of 1.0 bpm (0.159 m^3/min). The plastic viscosity (PV) is 40 cP, and the yield point (YP) is 0, for both fluids. Case 3 is in a horizontal pipe at a flow rate of 5 bpm (0.795 m^3/min), where the brown fluid is fluid C (PV = 40 cP, YP = 9.57 Pa) and the gray fluid is fluid B (PV = 80 cP, YP = 14.36 Pa). Note Case 2 has a fluid top lower than Case 1 and 3 because of free fall. In each plot, the gravity vector is drawn with a label "g" and the imposed velocity vector is shown with a label "u". The Reynolds numbers are 835, 835, and 112 for Case 1, 2 and 3, respectively.

and Newtonian fluids at different flow rates in a vertical pipe using the current model and show the results in Fig. 10. All snapshots show the time when the pumped volume of fluid is equal to a half of the pipe's interior volume. Because of yield stress and relatively high viscosity, the BP fluid is stably displaced under all flow rates, and the displacing fluid in the highest flow rate moves slightly ahead of the other two cases, owing to lower effective viscosity. As seen in Fig. 10b, all three cases of Newtonian fluid developed instabilities at the fluid interfaces, especially at the lowest flow rate. At the highest flow rate, although the fluid front shows blurred interface, the flow seems more stable and closer to its counterpart of BP flow, an expected result due to the stabilizing effect of high-velocity displacement flow (Amiri et al., 2016).

3.4. Field cases

Our in-pipe displacement model is combined with an annulus model (Dai and Liu, 2018) to simulate a cementing job as a continuous displacement process. The fluids moving out of casing interior at the bottom are assumed uniformly mixed, using their concentrations calculated from the in-pipe model, and then the annulus model uses the mixed fluids from the bottom as the inlet condition for annular simulation. The entire displacement process is simulated to consider multiple fluids are pumped sequentially including mud, prewash, spacer, slurries and displacement. The pipe eccentricity profile is calculated by a centralization model using the information of centralizer placement and is applied to the annulus displacement model. Two examples of real cementing jobs are simulated and presented in the following.

Case 1. This well is 10,630 ft (3240 m) in measured depth with an inclination angle of 21.5° at the casing shoe. The wellbore trajectory is shown in Fig. 11a. The previous casing was set at 9357 ft (2852 m), and the current job will cement the 9.625 casing in the open hole with diameters in the range of 12.2 in.–15.9 in (309.9 mm–403.8 mm). The pumping rate varies from 5 to 7 bpm (0.795–1.133 m^3/min). The well is meshed using a 100-ft (30.48-m)

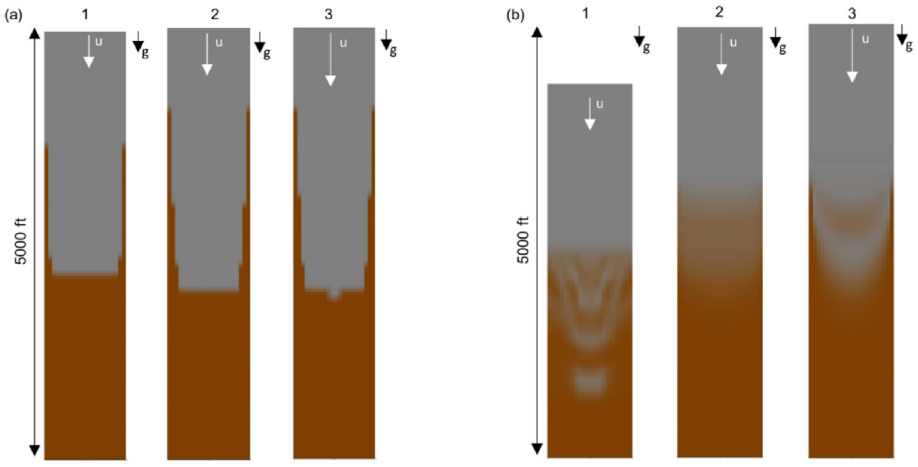

Fig. 10. Simulated displacement results using the current model for three cases with different flow rates (Case 1 to 3 are 0.159, 0.795, and 1.59 m^3/min, respectively). (a) Bingham Plastic fluids. The gray fluid is fluid B (PV = 80 cP, YP = 14.36 Pa) at 1437.8 kg/m3, and the brown fluid is fluid C at 1078.4 kg/m3 (PV = 40 cP, YP = 9.57 Pa). The Reynolds numbers are 4.6, 112, and 433 for Case 1, 2 and 3, respectively. (b) Newtonian fluids. The gray fluid is 1437.8 kg/m3, μ = 40 cP; and the brown fluid is 1078.4 kg/m3, μ = 40 cP. The Reynolds numbers are 835, 4177, and 8354 for Case 1, 2 and 3, respectively. The gravity vector is drawn in each plot with a label "g" and the imposed velocity vector is shown with a label "u".

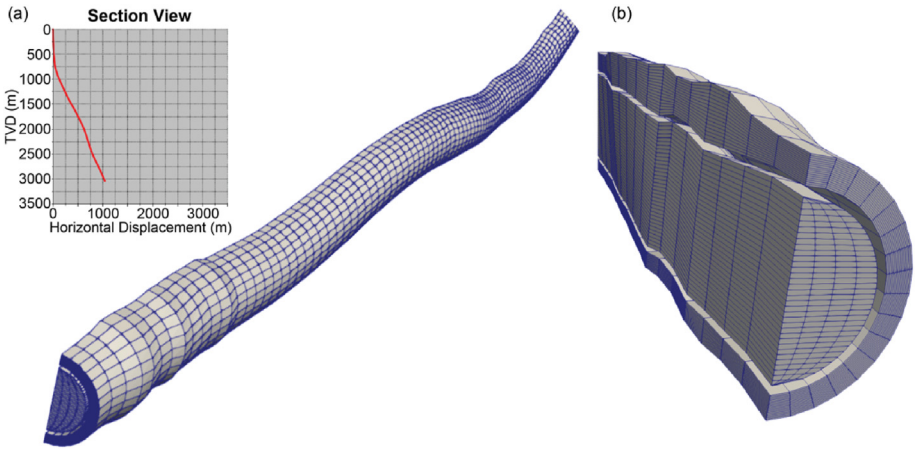

Fig. 11. Numerical simulation of a real cementing job using the current model. (a) Wellbore trajectory and the 3D mesh created for the full well simulation; (b) mesh detail near the bottom of the well (a cut view).

axial grid size for both in-pipe and annulus models, creating a 3D structured mesh of 43000 cells in total. Fig. 11b shows the exterior view and a cut view of the mesh. The time step size is 0.2 min. The displacement job is 299.1 min long, and the total computational time for the simulation is around 10 min on a regular PC (the same one as mentioned in section 3.1).

The displacement flow is visualized in Fig. 12a for results in both pipe and annulus at different moments. In each snapshot, the narrow side annulus and the wide side annulus are shown on the left side and right side, respectively, and the pipe interior is shown in the middle. In the beginning, the spacer enters the well with a symmetric interface. When arriving at the deviated section, the spacer slumps to the lower side in the pipe because of a density higher than the mud. The interface between the lead and tail slurries, however, was significantly mixed in the deviated section because of instability development, which is further developed after it enters the annulus. Contaminations of spacer are nearly absent inside pipe, but become significant in the annulus. Because a top plug is used to isolate the displacement and slurry, the mixing of the two is prevented. A 3D visualization of the fluids at 148.8 min is also shown in Fig. 12b.

We evaluate displacement efficiency by associating the simulated fluid concentrations in the annulus at the end of job with the CBL logs acquired during post-job evaluation. The standoff profile computed from the centralization model (Fig. 13a) is around 80% for cased hole, and above 50% in the open hole, which only affects the annulus displacement efficiency. Both the concentric model and the current model are used to simulate the job, and the results are seen in Fig. 13b and d, where the differences are attributed to in-pipe model only, given that the annulus displacement was simulated by the same annulus model. Significantly different top depths of tail cement are found. Based on the prediction of the new model, tail cement is absent above 7,500 ft (2286m), and its concentration in the lower section of the well greater than 8000 ft (2438 m) is much higher than that predicted by the concentric model. The concentric model predicted significant amount of both lead and tail slurries from around 6600 ft to 8000 ft (2012m–2438m), and the top of tail slurry goes to approximately 5500 ft (1676m). An intuitive explanation for this result is that the concentric model predicted earlier arrival of tail cement at the casing shoe from inside pipe than the new model. This is because the front of tail cement is largely moving at the center of the pipe, since segregation and mixing are absent, and the central part of fluid has a higher axial velocity. The prediction of the

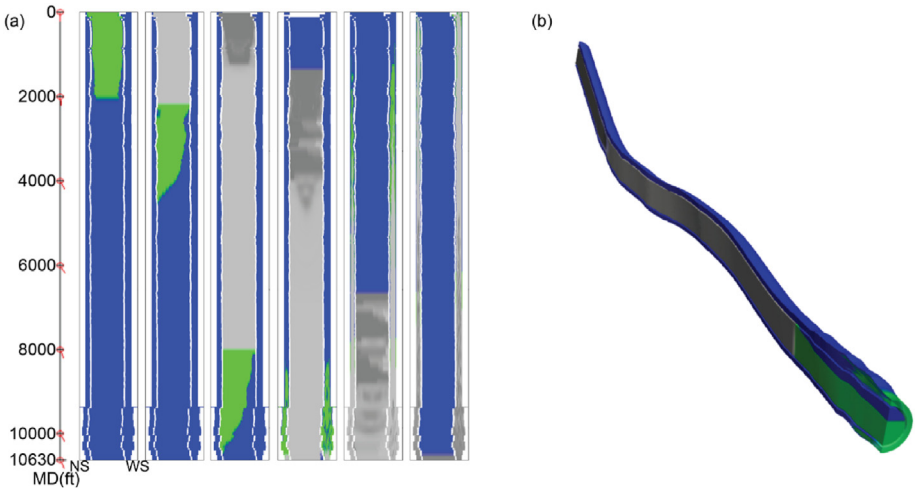

Fig. 12. Simulated snapshots of fluid displacement in pipe and in the annulus. (a) Cut view in 2D schematics. The corresponding times for each snapshot from left to right are t = 32, 60.7, 132, 180, 237.4, and 299 min; (b) cut view of 3D displacement at t = 148.8 min. The blue fluid is drilling fluid (1917 kg/m3), the green fluid is spacer (1953 kg/m3), and the light and dark gray fluids are lead and tail slurries (2001.0 kg/m3 and 2252.6 kg/m3, respectively).

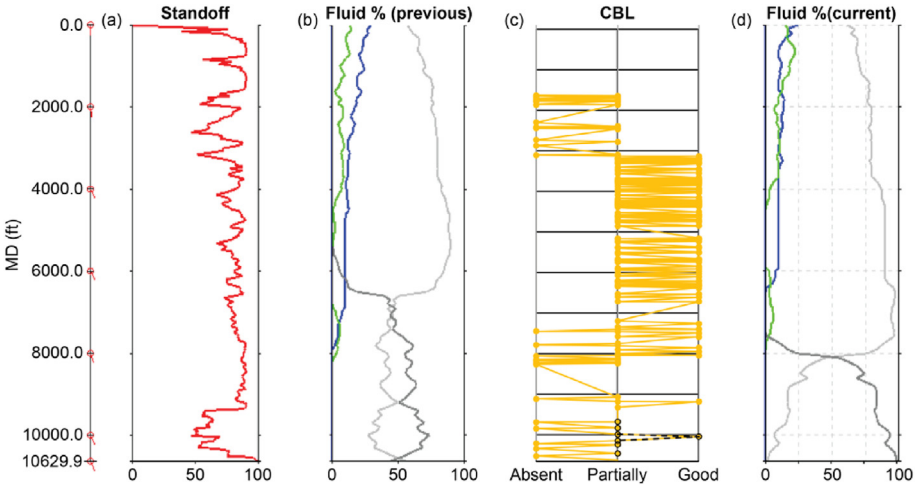

Fig. 13. Simulation result is compared to the evaluation logs from a real well. (a) The calculated standoff profile for the annulus displacement simulation; (b) the final fluid concentrations in the annulus predicted by the concentric model, where the mud, spacer, lead slurry and tail slurry are represented by blue, green, light gray and dark gray lines, respectively. (c) The CBL result acquired in job evaluation for the actual well, where yellow line with dots and black line with empty black circles show the cement bond to casing and to rock, respectively. (d) The simulated annular fluid concentrations predicted by the new model, where the lines are the same representations as in (b).

new model is more consistent with the CBL result shown in Fig. 13c, where we see good or partial contact to the casing above 7,500 ft (2286 m) without complete loss of contact. Compatibility tests show that lead and tail cements can mix to form a low viscosity mixture, contributing to less effective displacement and poor mud removal on the casing side and rock side. Hence, the cement bond quality in lower section greater than 8000 ft (2438 m) in this well is not satisfactory.

Case 2. The job is to cement an intermediate casing for a well at a measured depth of 825m (TVD = 473m), where it reaches the horizontal section. A surface casing of 387.3 mm in ID has been cemented at 215 m. The current casing is 298.4 mm in OD and 276.3 mm in ID. The open hole has a large annular excess of 92%, estimated from the pumped and returned cement volumes. Because of the large annular clearance, it is difficult to perform an effective mud displacement. The drilling fluid is 1090 kg/m^3, and the fluid sequence in the pumping order is water, viscosified Potassium Silicate wash (1260 kg/m^3), bottom plug, water, scavenger (1300 kg/m^3), top plug, cement (1725 kg/m^3), and water (displacement fluid). All fluids except cement are less viscous than the mud, resulting in significant mixing between the mud and these fluids and among these fluids inside both the pipe and the annulus. There was also significant mixing between the cement and leading fluids inside pipe, as found from the post-job simulations. The actual job had 109.3 m^3 cement pumped and 52 m^3 good cement returned to surface. Although the pumped cement volume is nearly twice of the annulus volume, the eventual displacement efficiency disclosed by cement evaluation logs was not satisfactory. The previous casing shoe was not securely bonded, and the previous cased hole above 215 m was mostly unbonded (Fig. 14a). The numerical result by the current model with inside pipe simulation consistently reveals lower cement concentration (Fig. 14b) above

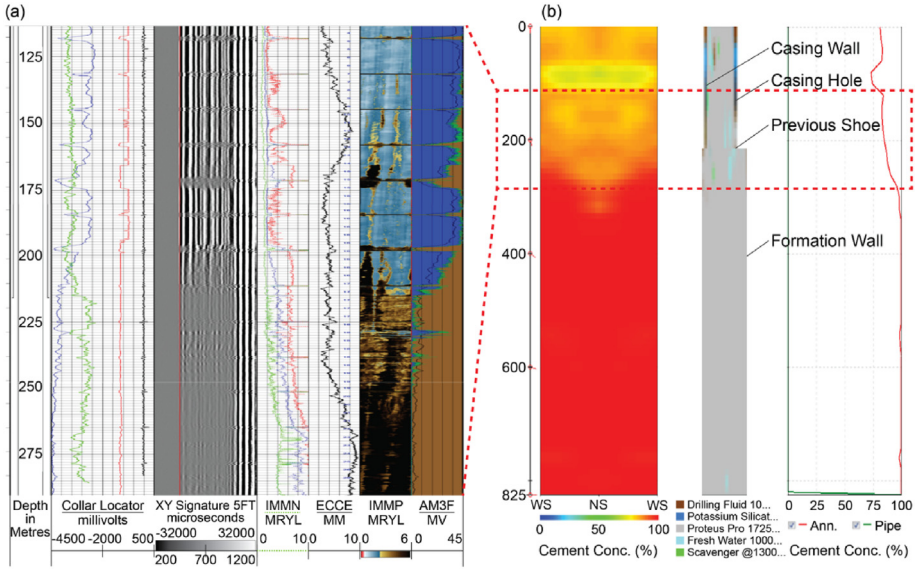

Fig. 14. Cement evaluation logs and simulated displacement efficiency at the end of the job. (a) Cement logs from 115 m to 290m including CBL (amplitude in blue, gamma ray in green, and travel time in red), VDL, and acoustic impedance image, (b) from left to right, simulated azimuthal cement concentrations in the annulus, radial cut-off view of the annular fluid distribution, annular cement percentage. The cut-off view shows poor contact on the casing wall and formation wall above the previous casing shoe.

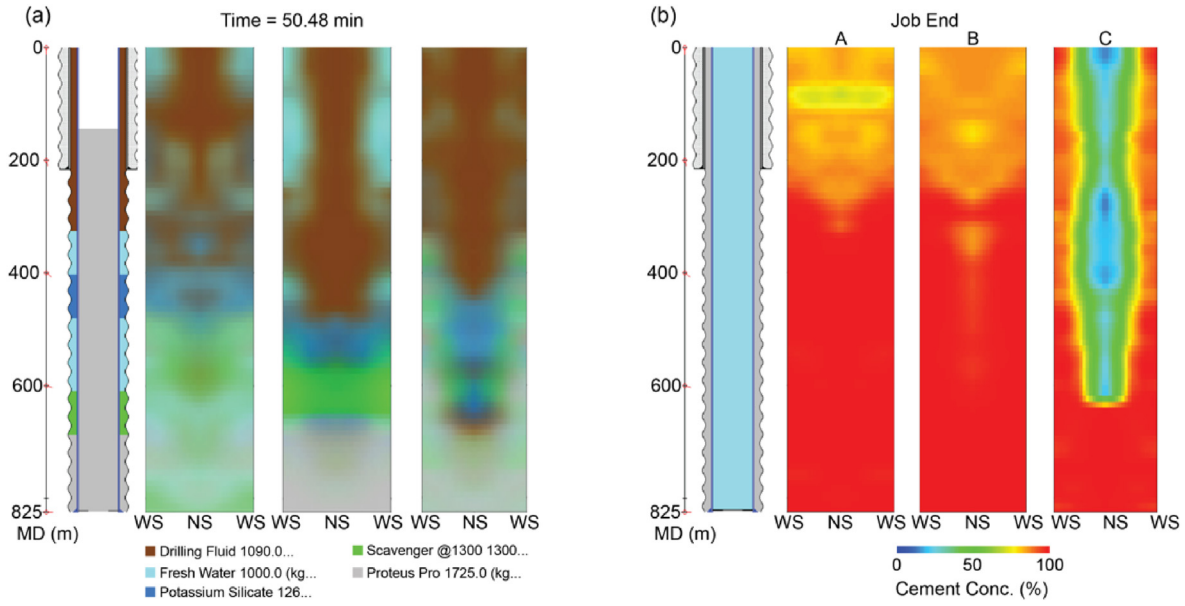

Fig. 15. A comparison of simulation results for the job. (a) Simulated annular fluid distributions at time = 50.48min, or when the ideal cement front reaches approximately 700 m in the annulus and, (b) simulated annular cement coverages at the end of job. In both (a) and (b), the four image tracks from left to right are wellbore schematic showing ideal fluid fronts, simulation by the current model (A), simulation without inside-pipe mixing (B), and simulation with the concentric model (C), respectively.

the previous shoe and apparent fluid layers existing on the casing wall and the formation wall, as found in the cut view of the annulus (in the middle of Fig. 14b).

The low displacement efficiency is mainly caused by the rheological relationship between the displacing and displaced fluids. Thin fluids pumped before cement actively penetrates in the native mud and mixes with it, causing azimuthal channels (Fig. 15a). The channels and most mixed fluids were displaced out of the well after a large volume of cement pumped into the annulus, except in the result predicted by the concentric model (labeled by C in Fig. 15a and b), where a large length of uncemented channel was left over at the end of the job. If fluid mixing inside pipe is not simulated, or 100% displacement efficiency is assumed, which is possible only if separators are used, the cement and scavenger are much more stably displaced in annulus, as shown in the middle of Fig. 15a (labeled by B). Based on the simulation of the new model, the cement and the leading fluids are intensively mixed inside pipe. Nevertheless, after a large amount of cement is pumped, the final cement concentration is close to the result of the simulation without in-pipe mixing (Fig. 15b).

4. Conclusions

In this paper, we presented a new model for simulating displacement efficiency in a full-length pipe string for practical cementing applications. The model accounts for a higher level of flow complexity than the existing concentric model, through a solution of fluid flow, fluid transport, degrees of fluid mixing, and flow segregations. We explained the method, and presented validations against CFD results, laboratory test results and through a series of test studies. Two field cases of cementing jobs have been simulated and compared to cement evaluation logs. Based on testing results and case studies, the present model shows significant improvement from previous concentric model and satisfactory match to real displacement flow. The computer solution is efficient and can be used for full-length wellbore simulations of fluid displacement. This model can be further improved in two aspects: (1) improving the computational method of axial velocity profile, considering arbitrarily distributed fluids in a cross section; (2) applying partial mixing within the cross section using improved determination of interfacial instabilities, covering the effects of viscosity difference and yield stress.

Declaration of competing interest

The authors declare that they have no competing interests.

Acknowledgement

The experimental part of this research has been carried out at Laval University under the supervision of S.M. Taghavi, to whom the authors are grateful. This work was supported financially by the MITACS Accelerate International (Grant No. FO123977), providing a postdoctoral fellowship to A. Eslami.

Nomenclature

f_i	volume fraction of fluid
ig	gravitational acceleration
h	gap width
h_i	gap width at grid layer
ik	consistency index
m	viscosity ratio
n	flow behavior index
p	pressure
r	radial coordinate
u	axial velocity
u	mean axial velocity
u	velocity vector
v	azimuthal velocity
v_r	rotational velocity
v_t	inertial velocity
s	mixing status
z	axial coordinate
A	area
At	Atwood number

D	pipe diameter
D_m	macroscale diffusion coefficient
Fr	Froude number
L	length
Q	flow rate
R	pipe radius
Re	Reynolds number
Re_c	Critical Reynolds number
Re_t	Inertial Reynolds number
β	inclination angle
μ	viscosity
ω	angular velocity
ρ	density
ρ_h, ρ_l	density of heavy, density of light fluid
ρ_1, ρ_2	density of displaced fluid, density of displacing fluid
τ_w	shear stress on the wall
τ_o	yield stress
Δ t	time step
Δx	grid size

Appendix A. Model

A.1 Solving axial velocity

Pressure is assumed uniform within any cross section; hence, the axial pressure gradient $\frac{dp}{dz}$ is a function of axial position (denoted by z) only:

$$\frac{dp}{dz} = f(z), \tag{A.1}$$

The total flow rate $Q(z)$ at any given depth z is an integral of axial velocity $u(\mathbf{r})$, expressed by

$$Q(z) = \int_A u(\mathbf{r}) dA, \tag{A.2}$$

where $\int_A$ represents the integral over the cross section. Eqs (1) and (2) are essentially the simplified momentum and continuity equations, respectively, that govern a parallel axial flow in the pipe. Once the relationship between pressure gradient $\frac{dp}{dz}$ and the velocity distribution $u(\mathbf{r})$ is established, which will be discussed later, Eqs. (1) and (2) are solved simultaneously for $f(z)$, provided $Q(z)$ is known. This is done using an iterative process, namely, the Brent's root finding algorithm (Brent, 1971). When concentric profile is assumed, averaged rheological parameters and density of fluids are used to find the velocity profile. This greatly alleviates the difficulty of solving a two dimensional velocity profile. In the present method, the following equations are first used to find the velocity distribution along a radial line before applying it to the entire section axisymmetrically:

$$u(r) = A\left[\frac{T(r)}{k}\right]^{\frac{1}{n}+1} + B, \tag{A.3}$$

where

$$T(r) = \frac{\tau_w}{R} r - \tau_o \tag{A.4}$$

$$A = -\frac{k}{\left(\frac{1}{n}+1\right)\frac{\tau_w}{R}} \tag{A.5}$$

$$B = \left[\frac{T(R)}{k}\right]^{\frac{1}{n}+1} \frac{k}{\left(\frac{1}{n}+1\right)\frac{\tau_w}{R}}. \tag{A.6}$$

In Eqs. (4)–(7), $u(r)$ is the axial velocity, τ_w is the shear stress on the wall, R is the inner radius of the pipe, r is the radial coordinate, and B the center velocity at $r = 0$. One can simply set T(r) = 0 when T(r) < 0 is found, because the velocity inside the unyielded plug zone will match the velocity at the plug boundary. Note the frictional pressure drop P satisfies

$$\mathrm{P} = \frac{dp}{dz} - \rho\, \mathrm{g} \cos\beta = \frac{2\tau_w}{R} \tag{A.7}$$

where β is the inclination angle (0° represents the vertical position), ρ is fluid density, and g is gravity acceleration. Very similar equations as Eqs. (4)–(7) are used for calculating the flow in annulus (assuming parallel plates) in the work by Dai and Liu (2018), but note that we have $\tau_w = \frac{h}{2}P$ for flow between plates with a gap width h, yet we have $\tau_w = \frac{R}{2}P$ for flow in a circular pipe.

For velocity in segregated flow, the horizontal distribution of the velocity in each layer is computed with Eqs. A.3-6 with R substituted by local half width $\frac{h_i}{2}$ as shown in Fig. 3a, which is possible because uniform fluid is considered in each layer. In the end, the horizontal profiles are adjusted using the vertical centerline profile as a guideline.

A.2 Solving fluid transport

The macroscopic diffusion coefficient can be in the order of 10^{-4} to 10^{-3} m^2/s for many experimental displacement flows in pipe, according to previous studies (Debacq et al., 2003; Alba et al., 2013a). In this step, we ignore the macroscopic diffusion, and we only consider incompressible flow, then Eq. (9) can be written in the following integrated form:

$$\frac{\partial}{\partial \mathrm{t}} \int_V f_i dV + \int_s \mathrm{u_n} f_s \, dS = \mathbf{0} \tag{A.8}$$

where the integral $\int_V$ is applied over a control volume, and $\int_s$ is applied over the boundary (surface) of the control volume. The u_n and f_s are the normal velocity and concentration value on the boundary faces. Eq. A.8 is solved using finite volume method, and an explicit Euler scheme for time integral is employed. Assuming uniform distribution of fluid concentration in the volume and on each face will lead to the following discretized equation, which is used to update the fluid concentration field:

$$f_i^{n+1} = f_i^n + \frac{\Delta t}{\Delta V} \sum_j \mathrm{u}_{n,j}^n f_{s,j}^n \tag{A.9}$$

where the superscripts n and $n+1$ represent the time steps, ΔV is the volume of the control volume, and Δt is the time interval. The current model does not calculate transverse velocity; therefore, the fluid is transported in axial direction only. Sharp interface is

maintained by applying axial interface reconstruction to suppress numerical diffusion because of large axial grid size. Consider a typical simulation of a cementing job with a time step of 0.1 min and a grid size of 30m, the numerical diffusion ($D_{m,n}$) is on the order of $D_{m,n} = \frac{\Delta x^2}{\Delta t} = 150\ m^2/s$, which is much greater than the diffusion coefficient D_m.

A.3 Fluid mixing and segregation

In this model, mixing of two or more fluids is first detected by checking interfacial instabilities and turbulence. Onset conditions of buoyancy-induced interfacial instabilities for density-unstable flow is investigated by previous experimental studies (Alba et al., 2013a; Amiri et al., 2016; Etrati and Frigaard, 2018a). This type of instabilities is considered absent for density-stable flow. The first flow regime we check is the diffusive mixing, which drives instantaneous displacement. The onset condition is when the following equation is satisfied:

$$\mathrm{Re}\cos\beta > 500\,\mathrm{Fr} - 50\mathrm{Fr}^2 \tag{A.10}$$

Mean viscosity $\mu_m = \sqrt{\mu_1\mu_2}$ is used to calculate the Reynolds number Re (Etrati and Frigaard, 2018a), where μ_1 is for displaced fluid and μ_2 for the displacing fluid. In the current model, viscosity is calculated by

$$\mu = \tau_0\frac{D}{u} + k\left(\frac{u}{D}\right)^{n-1} \tag{A.11}$$

and the Reynolds number Re and Froude number Fr are defined by

$$\mathrm{Re} = \frac{\rho u D}{\mu_m} \tag{A.12}$$

and

$$\mathrm{Fr} = \frac{u}{v_t}, \tag{A.13}$$

where v_t is the inertial velocity (Eq. (4)). The Reynolds number Re has a wide range from below 10 to above 10^6 in real cementing problems (using inlet velocity). A practical range of the Froude number Fr is 0.1–10.

The non-diffusive inertial regime is considered unstable, which drives fluid mixing if a time is given for instability growth. The inertial instability can cause complex, distorted, non-uniform fluid distribution. For cementing applications, because we consider long pipes, which will allow sufficient time for instability growth, we ignore the time of instability development and apply instantaneous mixing when this instability is detected, in the same way as the diffusive mixing. This is predicted by the following criterion (Taghavi et al., 2011)

$$\mathrm{Re}\cos\beta > 58.16\ \mathrm{Fr}^2 \tag{A.14}$$

A result of lubrication model, the Eq. A.14 can be used to predict backflows; it also defines boundary between the viscous regime and inertial regime for the region Fr > 1. At smaller *Fr*, we see exchange flows and the following condition is used as the boundary of instability (Séon et al., 2005):

$$\frac{\mathrm{Re}\cos\beta}{\mathrm{Fr}} > 50 \tag{A.15}$$

This criterion is established for iso-viscous displacement. Further studies on viscosity effect obviously imply a change of the regime boundaries based on viscosity ratio (Etrati and Frigaard, 2018a). For higher viscosity ratios, defined as $m = \mu_1/\mu_2$, the regime is expanded towards larger Fr and lower Re. Thus, the flow becomes more unstable than iso-viscous flow. Given that the effect is not well established for a wide range of Froude and Reynolds number, our current model ignored the impact of viscosity ratio in detecting instabilities.

Finally, turbulent flow is determined by

$$\mathrm{Re} > \mathrm{Re}_c = 2100 \tag{A.16}$$

Alternatively, the critical Reynolds number for Hershel-Buckley fluid can also be calculated by the method of Merlo et al. (1995).

In this model, we evaluate the criteria of instabilities for each section of depth using effective fluid parameters, which are calculated using averaged or dominant fluids at that section. No treatment is needed if instabilities are not existing; otherwise, a process is enforced to mix all the fluids within the cross section. However, because our framework is built on a 3D grid, the model has a potential to handle local mixing within partial cross section instead of full mixing in the whole cross section, as long as the detection of instability can be refined to a local region, such as for Kelvin-Helmholtz instability.

Segregation. In a high-inclination well with stable displacement flow, displacing and displaced fluids with a density difference can form a stratified flow pattern with the low-density fluid on top of the high-density one. In this stratified flow, transverse buoyancy plays a role of stabilizing the flow. Fluid segregation is the basis of a lubrication model, which is a simplified approach for solving displacement flow in a channel or pipe. In our model, an inertia Reynolds number is first calculated by

$$Re_t = \frac{\rho v_t D}{\mu}, \tag{A.17}$$

and the stratified flow is determined by

$$Re_t > 1, \tag{A.18}$$

Which suggests that the buoyancy is dominant over the inertia from the imposed flow. When fluid segregation is confirmed, all fluids in a cross section is redistributed to form a segregated pattern with densities in ascending order from top to the bottom. This is done conveniently in a layer-type grid. Within the cross section, fluid is uniformly distributed within each horizontal layer. In this process, volumes of each fluid are conserved and all fluids preserve their mixed or unmixed status. Mixed fluids will first form a homogenous mixture and then get involved in this segregation process as a new fluid with its averaged density. Mixed fluids are not possible to recover to separated fluids, consistent to the physical phenomenon. After segregation, unmixed fluids can possibly occupy the same cell in the grid and keep their unmixed status. Fig. A.1 is an example of simulated displacement flow with two Newtonian fluids inside a horizontal pipe. The pipe diameter is 19 mm and the length is 5 m. The displacing and displaced fluids are 1021 kg/m3 and 1000 kg/m3, making a Froude number of 0.01.

With a smaller imposed velocity (Fig. A1a), reversed trailing-front movement (backflow) is observed.

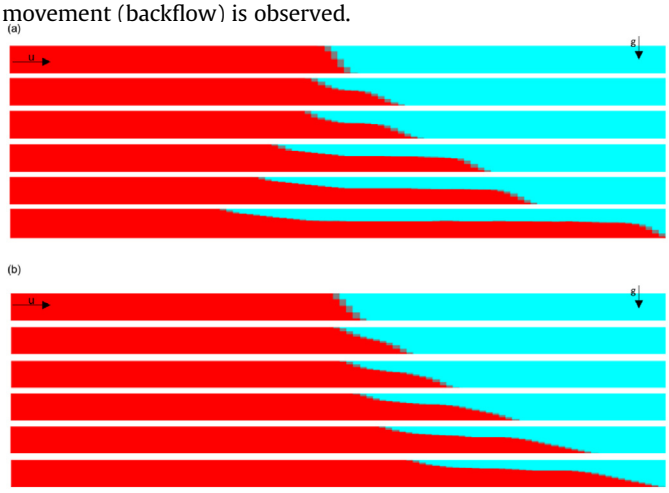

Fig. A.1. Simulated fluid interface evolution in a horizontal pipe at two different imposed velocities. The snapshots show the cut-off view through the pipe axis. The initial interface is in the middle of the pipe. The red fluid is the displacing fluid (1021kg/m3) and the cyan fluid is the displaced fluid (1000 kg/m3). The imposed flow is from left to the right. The inner diameter of the pipe is 19.05 mm. (a) Imposed velocity is 18.7 mm/s. The times are 0.019, 0.131, 0.169, 0.413, 0.581, 1.013 min. The trailing edge of the interface move backward. (b) Imposed velocity is 76 mm/s, where the trailing edge of the interface move forward. The times are 0.005, 0.055, 0.115, 0.171, 0.272, 0.369 min, respectively.

A.4 Tracking Mixed Fluids

The mixing status of fluids is tracked in three-dimensional space. We define a variable $s(\theta, z, r, t)$ to label this status at any position and time. Similar to the fluid concentration, the following condition is satisfied:

$$0 \leq s \leq 1, \tag{A.19}$$

where, $s = 1$ means fluid is fully mixed, and $s = 0$ means fluid is fully separable. This status variable evolves in time and also transports with the axial flow, by the following equation:

$$\frac{\partial s}{\partial t} + u\frac{\partial \boldsymbol{s}}{\partial x} = 0, \tag{A.20}$$

where $u = u(\theta, z, r, t)$ is the axial flow velocity. When solving Eq. A.20, we use similar techniques as in the VOF of fluid transport to track the interface. The solution of Eq.A.20 is used to check mixing status during fluid segregation, where $s < \frac{1}{2}$ is designated to represent unmixed fluids. After introducing this variable, two cells with equal fluid concentrations are not necessarily equivalent, causing different results of fluid segregation; mixed fluids are redistributed as an inseparable fluid with averaged density, yet unmixed fluids can be separated to different fluid layers. The current method continuously models the fluid regime change and transport during displacement. Fig. A2 shows an example of the displacement flow in a 5000 ft (1524 m) pipe (ID = 5 in., or 127 mm). The flow is stratified in the beginning, and after imposing an increase of velocity from 2 bpm (0.318 m^3/min) to 5 bpm (0.795 m^3/min), the two fluids fully mixed at the interface. Later, the mixed fluid further moves forward in a symmetric flow, which is not recovered to a stratified flow despite the imposed velocity is reduced to 2 bpm (0.318 m^3/min) again.

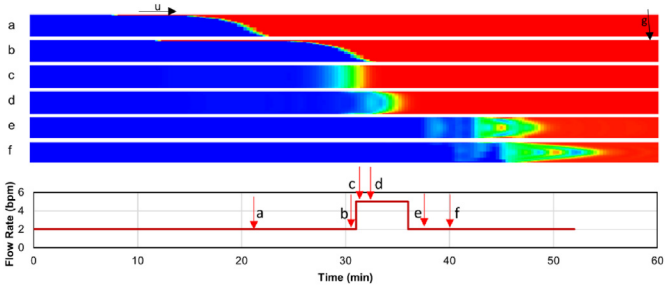

Fig. A.2. An example of flow regime evolution and transport simulated by the model. The pipe inclination is 85°. The times corresponding to (a)–(f) are 20.8 min, 30.6 min, 30.9 min, 31.7 min, 36.8 min and 40 min. The blue fluid (displacing fluid) is 1138.3 kg/m3, and the red fluid (displaced fluid) is 1078.3 kg/m3.

A.5 Other interfacial instabilities

In stratified flows, interfacial instabilities due to velocity difference between two layers or due to a viscosity jump can emerge (Etrati et al., 2018). The former is called Kelvin-Helmholtz instability, which introduces local mixing against buoyancy-induced segregation. This instability requires no viscosity difference and it even exists in inviscid flow. For K–H instability, Etrati and Frigaard (2018a) derived the following criterion using a two-layer model stability analysis:

$$\Delta u \leq \left[\frac{\pi}{2}\left(\frac{\rho_h - \rho_l}{\rho_h + \rho_l}\frac{gd^2}{S_i}\right)\sin\beta\right]^{\frac{1}{2}} \tag{A.21}$$

where Δu is the velocity difference between the two layers, ρ_h, ρ_l are densities of heavy and light fluids, and S_i is the interface length. In addition to K–H instability, a change of viscosity or friction force on the interface will promote unstable flow when the viscosity ratio is greater than 1 (i.e., thin fluid displaces thick fluid) and for small thickness of interface (Selvam et al., 2009). These two instabilities are considered to promote only local mixing near the interface and they are ignored in the present model for simplicity.

Appendix B. Experiments

B.1 Laboratory Setup

The testing facility is developed in the Department of Chemical Engineering, Laval University, Canada. Our experimental setup is a 3-m long circular pipe in a way that the pipe is mounted on a robust frame and the inclination angle can vary between horizontal and vertical (Fig. B1a). Two different circular pipes have been used, where inner diameters for the experimental tests are 9.6 mm and 19.05 mm. All the experiments are performed using two fluids (i.e., displacing and displaced fluids) in which the physical properties of the fluids (e.g., viscosity, density, yield stress value, etc.) can be changed to provide various density and viscosity contrasts. The pipes are transparent (plexiglass acrylic pipes) for flow visualization. In order to separate completely a displacing fluid and a displaced fluid before running each experiment, a gate valve (VAT, Inc.) is used to split the pipe to two parts (see both Fig. B1a and the schematic of the setup is shown in Fig. B1b.). To avoid pump disturbances, an elevated tank filled with the heavier fluid is employed where it is connected to the pipe and provides stable imposed flow, driven by gravity only. All the parameters are controlled by LabView, which can produce stable pipe rotations around its axis of

symmetry to simulate casing rotation. A low flow turbine flowmeter (OmegaFTB-420) and a needle valve placed before the drain are used to measure and control the flow rate. The pipe in testing is not a full-scale representation of real oil pipes, and non-dimensional groups of parameters of testing variables are considered to ensure similarity with real operations.

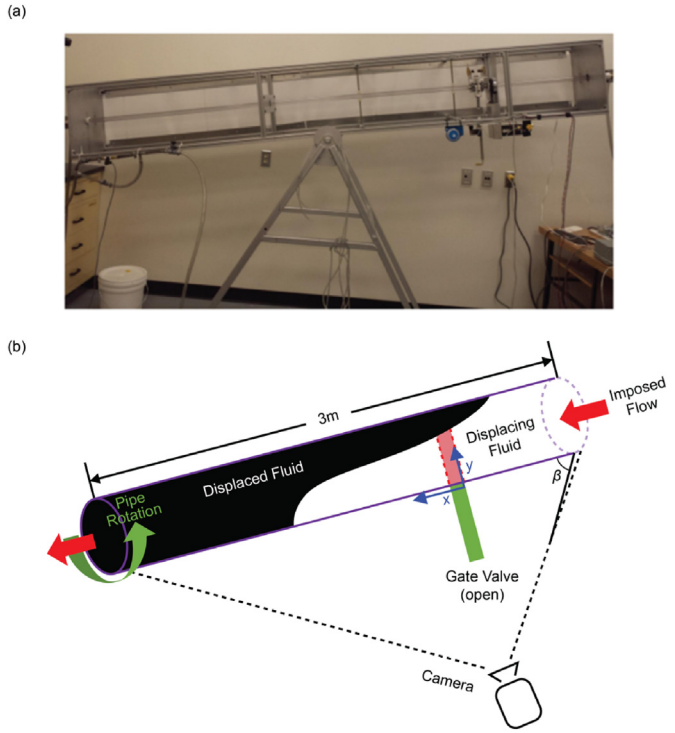

Fig. B.1. Experimental setup of the in-pipe displacement tests. (a) Real view of the laboratory setup of an inclined pipe. (b) Schematic of the displacement flow.

B.2 Testing Procedure

Two-fluid displacement flow experiments are conducted with fluids that have a yield stress. In order to mimic the behavior of the fluids involved in the industrial well cementing process, the test fluids are carefully prepared using polymeric powders including Carbopol (Carbomer 940, Making Cosmetics Co.) mixed with water, salt-water, Glycerin, Xanthan gum, etc., used as common transparent laboratory fluids. The Xanthan gum and Carbopol solutions are widely used to mimic shear-thinning and yield stress behavior in experimental studies of displacement flows. These solutions can exhibit non-Newtonian behavior quite similar to those of cement slurries and drilling muds. Salt-water solutions are used as heavy Newtonian fluid (displaced fluid) pushes a lighter yield stress fluid (Carbopol used as a displaced fluid colored by black ink for phase illustration). In a typical experiment, a displacing fluid is injected into the pipe to displace and remove the in-situ fluid. A high-speed camera records the evolution of the displacement flow to capture the advancement of fluid interfaces and record the concentration field of mixed fluids. The recorded images are post-processed using in-house MATLAB codes, ImageJ and the camera software.

Our experimental out-of-scale test flow loop can represent an approximately 100-ft (30 m) long full-scale pipe used in real cementing operation (consider a 9.625-in casing), allowing us to track the displacement front development, instability growth and displacement flow features. The experimental study covers a considerably wide range of pipe inclination, flow rate, density ratio, viscosity ratio, rheology parameters and rotation speed. Despite rich experimental results due to the effects of the aforementioned parameters variation, only part of which are presented in this paper for benchmarking the current model development.

References

Alba, K., Taghavi, S.M., Frigaard, I.A., 2012. Miscible density-stable displacement flows in inclined tube. Phys. Fluids 24, 123102.
Alba, K., Taghavi, S.M., Frigaard, I.A., 2013a. Miscible density-unstable displacement flows in inclined tube. Phys. Fluids 25, 067101.
Alba, K., Taghavi, S.M., de Bruyn, J.R., Frigaard, I.A., 2013b. Incomplete fluid–fluid displacement of yield-stress fluids. Part 2: highly inclined pipes. J. Non-Newtonian Fluid Mech. 201, 80–93. https://doi.org/10.1016/j.jnnfm.2013.07.006.
Amiri, A., Larachi, F., Taghavi, S.M., 2016. Buoyant miscible displacement flows in vertical pipe. Phys. Fluids 28 (10), 102105.
Aranha, P.E., Miranda, C., Cardoso Jr., W., Campos, G., Martins, A., Gomes, F.C., Araujo, S., Carvalho, M., 2012. A comprehensive theoretical and experimental study on fluid displacement for oilwell-cementing operations. In: SPE Deepwater Drilling and Completions Conference. Galveston, Texas, Society of Petroleum Engineers. https://doi.org/10.2118/150276-PA.
Braghini, A., Naccache, M., Fonseca, M., Miranda, C., Martins, A., Aranha, P., 2010. Effect of rheology on flow displacement during cementing process in oil wells. Proc. ENCIT, 13th Brazilian Congress of Thermal Sciences and Engineering, Uberlândia, MG, Brazil.
Bittleston, S., Ferguson, J., Frigaard, I., 2002. Mud removal and cement placement during primary cementing of an oil well – laminar non-Newtonian displacements in an eccentric annular Hele–Shaw cell. J. Eng. Math. 43 (2–4), 229–253.
Brent, R.P., 1971. An algorithm with guaranteed convergence for finding a zero of a function. Comput. J. 14, 422–425.
Chen, Z., Chaudhary, S., Shine, J., 2014. Intermixing of Cementing Fluids: Understanding Mud Displacement and Cement Placement. Society of Petroleum Engineers. https://doi.org/10.2118/167922-MS.
Chin, W.C., Zhuang, X., 2011. Transient, multiphase, three-dimensional pumping models for cementing and drilling. In: AADE 2011 National Technical Conference and Exhibition, Houston, Texas, USA.
Dai, H., Liu, G., 2017. Displacement demystified. Oilfield Technol. 2017 (3), 27–32.
Dai, H., Liu, G., 2018. An overview of annular displacement efficiency in cementing jobs using an efficient numerical model. In: AADE Fluids Technical Conference and Exhibition, Houston, Texas, USA.
Deawwanich, T., 2013. Flow and Displacement of Viscoplastic Fluids in Eccentric Annuli. The University of Adelaide, PhD thesis.
Debacq, M., Hulin, J.P., Salin, D., Perrin, B., Hinch, E.J., 2003. Buoyant mixing of miscible fluids of varying viscosities in vertical tube. Phys. Fluids 15, 3846–3855.
Enayatpour, S., van Oort, E., 2017. Advanced modeling of cement displacement complexities. In: SPE/IADC Drilling Conference.
Ermila, M.A., Eustes, A.W., Mokhtari, M., 2012. Using Magneto-Rheological Fluids to Improve Mud Displacement Efficiency in Eccentric Annuli. Society of Petroleum Engineers. https://doi.org/10.2118/160966-MS.
Eslami, A., Akbari, S., Taghavi, S.M., 2022. An experimental study of displacement flows in stationary and moving annuli for reverse circulation cementing applications. J. Petrol. Sci. Eng. 213, 110321. https://doi.org/10.1016/j.petrol.2022.110321.
Etrati, A., Frigaard, I.A., 2018a. A two-layer model for buoyant inertial displacement flows in inclined pipes. Phys. Fluids 30, 022107. https://doi.org/10.1063/1.5019366.
Etrati, A., Alba, K., Frigaard, I.A., 2018. Two-layer displacement flow of miscible fluids with viscosity ratio: experiments. Phys. Fluids 30, 052103. https://doi.org/10.1063/1.5026639.
Etrati, A., Frigaard, I.A., 2018b. Viscosity effects in density-stable miscible displacement flows: experiments and simulations. Phys. Fluids 30, 123104. https://doi.org/10.1063/1.5065388.
Feng, F., Ai, C., Yu, F., Cui, Z., Fan, S., Xu, H., 2013. The effects of density difference on displacement interface in eccentric annulus during horizontal well cementing. Open Petrol. Eng. J. 6, 79–87.
Foroushan, H.K., Ozbayoglu, E., Gomes, P.J., Miska, S., Yu, M., 2018. Mud-cement Displacement in Eccentric Annuli: Analytical Solution, Instability Analysis, and Computational Fluid Dynamics Simulations. Society of Petroleum Engineers. https://doi.org/10.2118/189646-MS.
Grasinger, M., Li, Z., Vuotto, A., Brigham, J., Iannacchione, A., Vandenbossche, J., 2015. Simulation of Cement Slurry Flow to Assess the Potential for Voids and Channels in Wellbore Cementing Processes. Society of Petroleum Engineers. https://doi.org/10.2118/177311-MS.
Joseph, D.D., Renardy, M., Renardy, Y., 1984. Instability of the flow of two immiscible liquids with different viscosities in a pipe. J. Fluid Mech. 141, 309–317.
Kiran, R., Salehi, S., Mokhtari, M., Kumar, A., 2019. Effect of Irregular Shape and Wellbore Breakout on Fluid Dynamics and Wellbore Stability. American Rock Mechanics Association.
Liu, G., 2021. Applied Well Cementing Engineering, first ed. Elsevier.
Maleki, A., Frigaard, I.A., 2017. Primary cementing of oil and gas wells in turbulent and mixed regimes. J. Eng. Math. 107 (1), 201–230.
Merlo, A., Maglione, R., Piatti, C., 1995. An innovative model for drilling fluid hydraulics. In: SPE Asia Pacific Oil & Gas Conference. Kuala Lumpur, Malaysia.
Moran, L., Savery, M., 2007. Fluid movement measurements through eccentric

annuli: unique results uncovered. In: SPE Annual Technical Conference and Exhibition, Anaheim, California, USA.
Nelson, E.B., Guillot, D., 2006. Well Cementing, second ed. (Schlumberger).
Pks, S., Yerubandi, K.B., 2010. Slim Well Completions: A 3D Numerical Approach for Displacement to Design Effective Cementing Fluids. Society of Petroleum Engineers. https://doi.org/10.2118/132480-MS.
Renteria, A., Maleki, A., Frigaard, I., Lund, B., Taghipour, A., Ytrehus, J.D., 2018. Displacement Efficiency for Primary Cementing of Washout Sections in Highly Deviated Wells. Society of Petroleum Engineers. https://doi.org/10.2118/191989-MS.
Sarmadi, P., Renteria, A., Thompson, C., Frigaard, I.A., 2022. Effects of wellbore irregularity on primary cementing of horizontal wells, Part 2: small scale effects. J. Petrol. Sci. Eng. 210, 110026. https://doi.org/10.1016/j.petrol.2021.110026.
Selvam, B., Talon, L., L, Lesshafft, L., Meiburg, E., 2009. Convective/absolute instability in miscible core-annular flow. Part 2. Numerical simulations and nonlinear global modes. J. Fluid Mech. 618, 323–348.
Skadsem, H.J., Kragset, S., Sørbø, J., 2019. Cementing an Irregular Annulus Geometry: Full-Scale Experiments and 3D Simulations. Society of Petroleum Engineers. https://doi.org/10.2118/194091-MS.
Séon, T., Hulin, J.P., Salin, D., Perrin, B., Hinch, E.J., 2005. Buoyant driven miscible front dynamics in tilted tubes. Phys. Fluids 17, 031702.
Taghavi, S.M., Seon, T., Wielage-Burchard, K., Martinez, D.M., Frigaard, I.A., 2011. Stationary residual layers in buoyant Newtonian displacement flows. Phys. Fluids 23, 044105.
Taghavi, S.M., Alba, K., Frigaard, I.A., 2012a. Buoyant miscible displacement flows at moderate viscosity ratios and low Atwood numbers in near-horizontal ducts. Chem. Eng. Sci. 69 (1), 404–418. https://doi.org/10.1016/j.ces.2011.10.065.
Taghavi, S.M., Alba, K., Seon, T., Wielage-Burchard, K., Martinez, D.M., Frigaard, I.A., 2012b. Miscible displacement flows in near-horizontal ducts at low Atwood number. J. Fluid Mech. 696, 175–214.
Tardy, P.M., Bittleston, S.H., 2015. A model for annular displacements of wellbore completion fluids involving casing movement. J. Pet. Sci. Eng. 126, 105–123.
Tardy, P.M., Flamant, N.C., Lac, E., Parry, A., Sutama, C., Almagro, S., 2017. New Generation 3D Simulator Predicts Realistic Mud Displacement in Highly Deviated and Horizontal Wells. Society of Petroleum Engineers. https://doi.org/10.2118/184677-MS.
Tehrani, M.A., Ferguson, J., Bittleston, S.H., 1992. Laminar displacement in annuli: a combined experimental and theoretical study. In: 67th Annual Technical Conference and Exhibition, Washington, DC.
Wang, Y., Dai, H., 2018. Parametric analysis of efficiency using an efficient mud displacement modeling technique. In: AADE Fluids Technical Conference and Exhibition, Houston, Texas, USA.
Weller, H.G., Tabor, G., Jasak, H., Fureby, C., 1998. A tensorial approach to computational continuum mechanics using object-oriented techniques. Comput. Phys. 12 (6), 620–631.
Xie, L., Chaudhary, S., Chen, Z., 2015. Analysis of the Effect of Eccentricity on Displacement of Non-newtonian Fluids with a Hybrid Method. Society of Petroleum Engineers. https://doi.org/10.2118/174909-MS.